Nanoscale

Accepted Manuscript

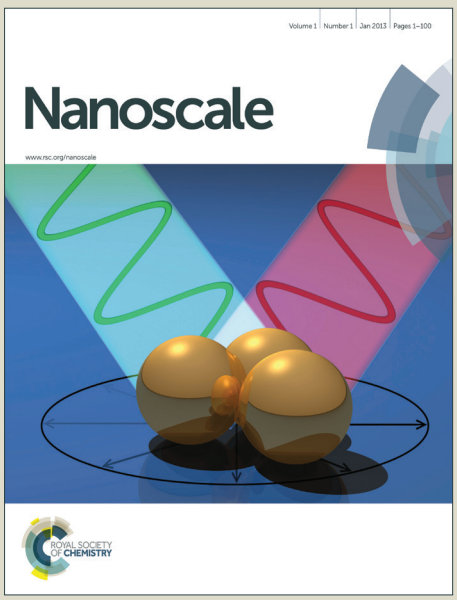

ROYAL SOCIETY OF CHEMISTRY

www.rsc.org/nanoscale

Journal Name

RSCPublishing

ARTICLE

Lignin-assisted exfoliation of molybdenum disulfide in aqueous media and its application in lithium ion batteries

Cite this: DOI: 10.1039/x0xx00000x

Received 00th January 2012,
Accepted 00th January 2012

DOI: 10.1039/x0xx00000x

www.rsc.org/

Wanshuang Liu,‡[a] Chenyang Zhao,‡[ab] Rui Zhou,[a] Dan Zhou,[a] Zhaolin Liu,[b] and Xuehong Lu*[a]

In this article, alkali lignin (AL)-assisted direct exfoliation of MoS_2 mineral into single-layer and few-layer nanosheets in water is reported for the first time. Under optimized conditions, the concentration of MoS_2 nanosheets in the obtained dispersion can be as high as 1.75±0.08 mg mL^{-1}, which is much higher than the typical reported concentrations (< 1.0 mg mL^{-1}) using synthetic polymers or compounds as surfactants. The stabilizing mechanism primarily lies in the electrostatic repulsion between negative charged AL, as suggested by zeta-potential measurement. When the exfoliated MoS_2 nanosheets are applied as electrode materials for lithium ion batteries, they show much improved electrochemical performance compared with the pristine MoS_2 mineral because of the enhanced ion and electron transfer kinetics. This facile, scalable and eco-friendly aqueous-based process in combination with renewable and ultra-low-cost lignin opens up possibilities for large-scale fabrication of MoS_2-based nanocomposites and devices. Moreover, herein we demonstrate that AL is also an excellent surfactant for exfoliation of many other types of layered materials, including graphene, tungsten disulfide and boron nitride, in water, providing rich opportunities for a wider range of applications.

1. Introduction

Recently, two-dimensional materials have attracted great attention owing to their high specific surface area and unique properties. Molybdenum disulfide (MoS_2), as a member of transition metal dichalcogenides, has a layered structure with a plane of Mo atoms covalently sandwiched between two planes of S atoms in a trigonal prismatic arrangement. MoS_2 is a good semiconducting material and possesses intrinsic band gap, which is the most attractive feature in comparison with gapless graphene.[1-3] MoS_2 exhibits unique electronic, optical and electrochemical properties, and has great potential for low-power electronics, optoeletronic devices, logic circuits, catalytic and energy storage applications.[4-9] However, just like graphene, the properties of MoS_2 are also thickness dependent. For example, bulk MoS_2 is an n-type semiconductor with an indirect band gap of ~1.2 eV, while single-layer MoS_2 is a direct-band gap semiconductor with a gap of ~1.8 eV.[2,6] Similarly, it has been demonstrated that the electrochemical charge storage capacity of MoS_2 nanosheets is much higher than that of bulk crystals owing to the larger surface area and more active edges of the former.[10-12] In order to utilize the valuable properties of monolayer or few-layer MoS_2, different exfoliation techniques or synthesis methods have been developed for MoS_2, including micromechanical exfoliation,[13] chemical exfoliation through intercalation,[14,15] liquid-phase exfoliation,[16] thermal ablation method,[17] chemical vapor deposition (CVD) on substrates[18] and direct solvothermal synthesis,[3] etc. Among these methods, liquid-phase exfoliation is so far the most suitable route for large scale production of MoS_2 nanosheets.[16] Although monolayer MoS_2 produced by scotch tape, CVD, etc. is ideal for electronics and optoeletronic devices, dispersed monolayer or few-layer MoS_2 produced by liquid-phase exfoliation will be sufficient to meet the requirements of a range of applications such as nanoscale hybrids for use in thermoelectrics, supercapacitors and lithium-ion batteries (LIBs).[19]

Liquid-phase exfoliation of MoS_2 in an aqueous media has economic and environmental advantages over the exfoliation in organic solvents.[20,21] The exfoliation of MoS_2 in water is, however, challenging owing to the its hydrophobic nature. One method to address this issue is to use surfactants, which allows the exfoliated sheets to remain suspended. So far a few types of block copolymers,[9] charged macromolecular[19,22] and small organic salts[23] have been used to stabilize exfoliated MoS_2 in water. This, however, requires tedious synthesis procedures, and the surfactants also have limited capability for dispersing MoS_2, giving dispersions with MoS_2 concentrations well below 1.0 mg mL^{-1}.

Lignin, the second most abundant natural polymer after cellulose, accounts for up to 20-30 wt% of wood.[24] The annual production volume of lignin by pulp and paper industry is

estimated to be 50 million tons.[25] Currently lignin goes mostly to relatively low-value energy recovery, so utilization of lignin in high-value products is receiving increasing attention. It is well known that the stabilization of surfactant-nanoparticle dispersions usually relies on electrostatic repulsion and/or steric hindrance.[23,26,27] Alkali lignin (AL), a type of low-cost commercial technical lignin, consists of negatively charged rigid macromolecules and is soluble in water.[28] Therefore, it has great potential to serve as surfactant for exfoliation of MoS_2 in aqueous media. In this work, AL was used as surfactant to prepare MoS_2 nanosheets in water by liquid-phase exfoliation method without any pre-treatment of MoS_2. Herein we report the effective exfoliation of bulk MoS_2 into nanosheets by this facile approach and the excellent stabilizing effects of AL. Under optimized dispersing condition, the obtained aqueous dispersions contain a concentration of MoS_2 as high as 1.75±0.08 mg mL^{-1}. To validate the usefulness of the exfoliated MoS_2 nanosheets, their electrochemical performances are demonstrated as both cathode and anode of LIBs. Our results also show that AL can be used as a general surfactant for direct exfoliation of a wide range of layered materials, including graphite, MoS_2, tungsten disulfide (WS_2) and boron nitride (BN) in aqueous media.

2. Experimental

2.1. Materials

MoS_2 (99% purity), WS_2 (99% purity) and hexagonal BN (98% purity) were purchased from Sigma-Aldrich Chemicals Inc. (USA). Alkali lignin (AL) was purchased from TCI America (USA, TCI product number: L0082, softwood lignin) and used without further purification. 1M $LiPF_6$ in a mixture of ethylene carbonate (EC) and dimethyl carbonate (DMC) at a 1:1 volume ratio were purchased from Charslton Technologies Pte Ltd (Singapore).

2.2. Exfoliation of MoS_2.

A desired amount of AL (25, 125, 250, 375 or 500 mg) was added to 250 mL Millipore water in a glass bottle. When AL was completely dissolved, 2.5 g bulk MoS_2 was added into the AL solution. The mixture was then sonicated in a low-power sonic bath (MRC product: DC200H, 200W) for 5 to 80 h. The resulting dispersions were left to stand for approximately 24 h to allow large unstable MoS_2 aggregates to form and then centrifuged for 15 min at 1500 rpm to remove unexfoliated MoS_2. After centrifugation, the top 40 mL (out of 50-mL centrifuge tube) was carefully removed by pipet and retained for further use.

The above AL-MoS_2 dispersion was vacuum-filtered onto a nitrocellulose membrane (Millipore, 0.025 μm pore size, 47 mm diameter) and washed with excess Millipore water. The obtained solids were re-dispersed in a small amount of water by bath sonication for 2 h. The undispersed fraction was removed by centrifugation at 1500 rpm for 15 min to give the saturated AL-MoS_2 dispersion without free AL.

2.3. Determination of MoS_2 concentration

A precisely measured 50 mL of AL-MoS_2 dispersion was filtered under high vacuum onto a pre-weighed nitrocellulose membrane (Millipore, 0.025 μm pore size, 47 mm diameter). After washing with excess Millipore water, the membrane was dried in a vacuum oven at 40 °C for 24 h and reweighed to give the deposited mass. Because it's impossible to thoroughly wash out the adsorbed AL, the content of MoS_2 mass on the filter membrane was determined by thermal gravimetric analysis (TGA).

2.4. Annealing of MoS_2 for LIBs application.

The saturated AL-MoS_2 dispersion without free AL was immersed in liquid nitrogen, followed by freeze-drying for 3 days. The obtained MoS_2 powder was annealed at 700 °C for 2h in an argon atmosphere.

2.5. Characterization

Optical absorption spectra were recorded on a Shimadzu UV-3600 UV–vis–NIR spectrophotometer with optical grade quartz cuvettes. For the MoS_2 dispersions with different lignin concentration, corresponding lignin aqueous solutions were scanned as baseline. All dispersions were diluted to one fifth or one twentieth of original concentrations because with the original concentrations the measured absorbance values for some samples exceed the measuring range of the equipment. Zeta potential and size distribution of the exfoliated MoS_2 were determined by dynamic light scattering (DLS) technology using a Zetasizer Nano ZS (Malvern Instruments Ltd., UK). All the samples for zeta potential measurements were tested at room temperature and PH value of 7.5. TGA was performed on a TA Instruments TGA Q 500 under a nitrogen atmosphere at a heating rate of 10 °C min^{-1}. Transmission electron microscopy (TEM) was performed on JEOL-2010 with accelerating voltage of 200 kV. Samples for TEM were prepared by dropping diluted MoS_2 dispersion on carbon-coated Cu grids. SEM observation was investigated by JEOL FESEM 7600F field emission scanning electron microscope. The samples were coated with gold for 60 s. Atomic force microscope (AFM) observation was conducted on a Dimension 3100 AFM (Digital Instruments). The MoS_2 dispersion without free AL was used in the AFM tests because residual free AL would disturb the measured thickness. The samples were prepared by spin-coating the diluted MoS_2 dispersion onto freshly cleaved mica. Raman spectra were obtained using a Renishaw Invia Raman microscope with an excitation wavelength at 633 nm. X-ray diffraction (XRD) patterns were recorded in a Bruker D8 Advanced XRD using Cu Kα radiation. X-ray photoelectron spectroscopy (XPS) measurements were performed on a Kratos Analytical AXIS His spectrometer with a monochromatized Al Kα X-ray source (1486.6 eV photons). The samples are tested with the MoS_2 powders obtained by freeze-drying the MoS_2 dispersion without free AL.

2.6. Electrochemical measurement

The electrochemical performances of the aqueous exfoliated MoS_2 were evaluated with a standard CR2032 coin cell. The working electrodes were composed of 60 wt% MoS_2, 30 wt% carbon black and 10 wt% polyvinylidene fluoride unless otherwise specified. A Celgard® 2600 membrane was used as the separator. Lithium metal foil was used as the counter/reference electrode, and 1 M $LiPF_6$ in a mixture of EC and DMC (1/1 in v/v) as the electrolyte. The cells were cycled between 1 ~ 3V and 0.01 ~ 3V vs Li/Li^+, respectively. The cyclic voltammetry (CV) was studied on a PGSTAT302N Autolab electrochemical workstation with a scan rate of 0.05 mV/s. For comparison purpose, the electrochemical performance of commercial MoS_2 powder (< 2μm) were tested under the same conditions.

3. Results and discussion

3.1. Lignin-assisted exfoliation of MoS_2

Stabilizing effects of AL on MoS_2. Lignin has a rigid, hyperbranched macromolecular structure composed of three different types of phenylpropane units and various functional groups such as hydroxyl, methoxy, ether, aldehyde, and ester groups (Fig. 1a).[24] The inset in Fig. 1a and Fig. 1b show the representative photographs of AL powder, AL and AL-MoS_2 aqueous dispersions (AL feed concentration of 0.5 mg mL^{-1}). The dark green AL-MoS_2 dispersion is prepared by sonication (5h) followed by centrifugation (1500 rpm for 15 min). This dispersion is very stable and only little sedimentation is observed over weeks. To explain the excellent aqueous stability, zeta potential of the AL and AL-MoS_2 aqueous dispersions was measured. The results (Fig. 1c) show that the dispersed AL and AL-MoS_2 are both negatively charged, with zeta potential of -42 and -37 mV, respectively. The values well exceed the accepted value for a stable colloid (-25 mV).[26] TGA analysis (Fig. 1d) shows that AL cannot be completely removed from Al-MoS_2 even after extensive washing, suggesting the adsorption of AL on the surface of exfoliated MoS_2 during the ultrasonic processing. Thus the high surface charge of AL makes the exfoliated MoS_2 stably suspended in the aqueous dispersion through electrostatic repulsion, as illustrated in Fig. 1e. It is noteworthy that, similar to other polymer surfactants, steric hindrance may also play a role in stabilizing exfoliated MoS_2 since AL consists of rigid macromolecules.[9,27]

Disperse condition. The effect of dispersion condition on the concentration of exfoliated MoS_2 (C_M) was investigated by UV-vis spectroscopy. Figs. 1f and 1g show the UV-vis spectra of diluted AL-MoS_2 aqueous dispersions with different AL feed concentrations and sonication time (feed concentration of bulk MoS_2 was fixed on 10 mg mL^{-1}). The spectra of the diluted AL-MoS_2 aqueous dispersions show two peaks at ~ 630 nm and 670 nm, which are related to the characteristic A1 and B1 direct excitonic transitions of MoS_2 with the energy split from valence band spin-orbital coupling.[9,18] According to the Lambert-Beer law ($A = \alpha C_M l$, where A is the absorbance, α the absorption coefficient, and l the path length), the C_M is proportional to optical absorbance A. It can be clearly seen that the C_M values monotonously increase with the AL feed concentration when the sonication time is 5 h (Fig. 1f). This result is in accordance with the reported study using copolymer and sodium cholate as surfactants.[9,19] However, when the sonication time is extended to 80 h (Fig. 1g), the C_M value no longer show monotonous increase with AL feed concentrations. The C_M values at different AL concentrations become fairly close to each other except the low C_M value obtained at the AL concentration of 0.1 mg mL^{-1}, and the maximum C_M value appears at the AL concentration of 1.0 mg mL^{-1}. The maximum C_M was measured to be 1.75±0.08 mg mL^{-1} according to the method described in the experimental section and TGA results of bulk MoS_2, AL, and AL-MoS_2 powders (Fig. 1d). This concentration is significantly higher than the reported C_M values obtained by liquid-phase exfoliation in aqueous media without prior treatment of MoS_2, as summarized in Table S1 in ESI†. However, it should be noted that concentrations reported in the

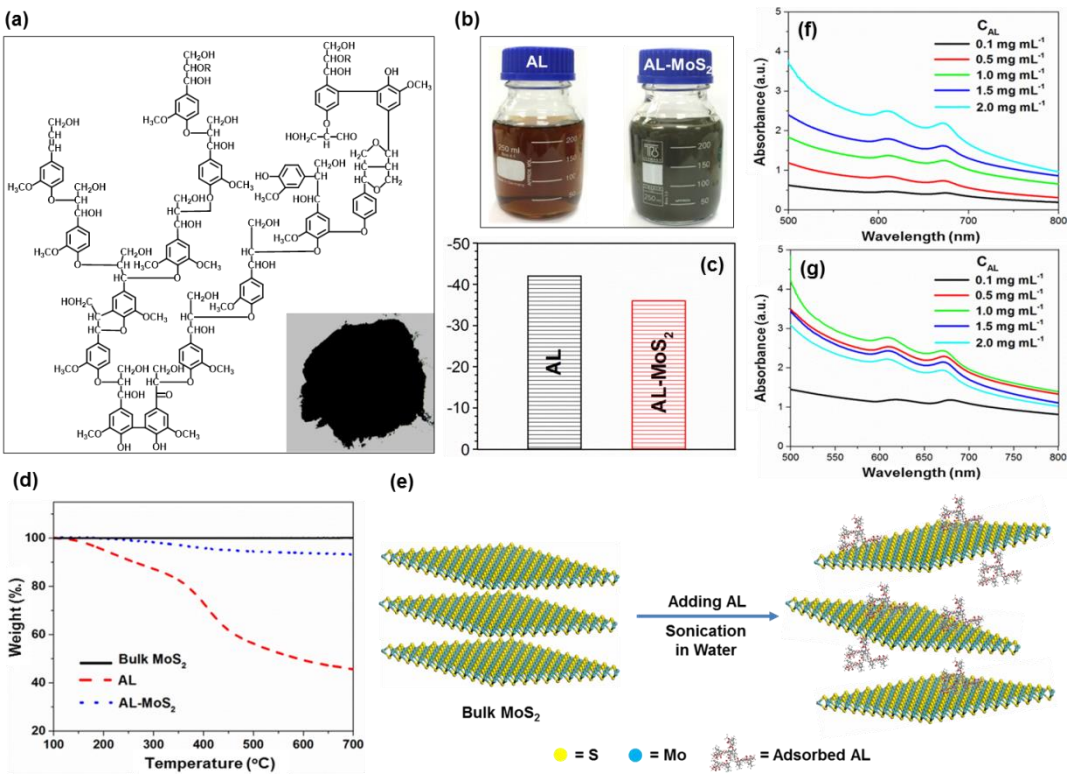

Fig. 1 (a) Structural model of lignin from ref 24. The inset shows the photograph of AL powder. (b) Photographs of AL and corresponding AL-MoS_2 aqueous dispersions. (c) Zeta potential of AL and AL-MoS_2 dispersion. (d) TGA curves of bulk MoS_2, AL and AL-MoS_2 (without free AL) powders. (e) Schematic illustration of the exfoliation of bulk MoS_2 and stabilization of the exfoliated MoS_2 by AL. UV−visible spectra of AL-MoS_2 aqueous dispersions with different AL feed concentrations. (f) Sonication treatment for 5 h (1/5 of original concentrations). (g) Sonication treatment for 80 h (1/20 of original concentrations).

cited references may be not the optimal values because the experimental parameters (such as ultrasonic time, centrifuge speed and time) would greatly affect the obtained product concentration.

Evidence of exfoliation. To investigate the disperse state of exfoliated MoS_2 in the aqueous dispersion, transmission electron microscopy (TEM) studies were conducted. The sample with AL feed concentration of 1.0 mg mL^{-1} and 80 h sonication treatment was chosen for the structure characterization. Fig. 2a and 2b show TEM images of typical MoS_2 nanosheets with lateral size > 100 nm collected from the MoS_2 aqueous dispersion. The MoS_2 nanosheets are slightly transparent to the electron beam and show low contrast with the carbon coating, indicating their ultrathin feature. The high-resolution TEM image in Fig. 2c shows the edge of a tri-layer MoS_2 nanosheet. High-resolution TEM image (Fig. 2d) reveals that the lattice structure of the MoS_2 nanosheet was not damaged during the exfoliation process. The electron diffraction pattern (inset in Fig. 2d) shows that the MoS_2 nanosheet exhibits high crystallinity.

Atomic force microscopy (AFM) was used to determine the thickness of the exfoliated nanosheets. The results reveal that the majority of the exfoliated MoS_2 are multilayer. Fig. 3a shows two typical MoS_2 nanosheets with thickness of 3.2 and 4.9 nm, respectively, which can be considered to consist of 3-5 atomic layers. Only few monolayer nanosheets are observed. As shown in in Fig. 3b, the thickness of the nanosheet shown is ~ 0.8 nm, which agrees with the typical height of a single-layer MoS_2 (0.6 – 1.0 nm).[29] SEM observation of the exfoliated MoS_2 powder without free AL (Fig. 3c) shows that nanosheet morphology can be well maintained after freeze-drying. The size distribution of the exfoliated MoS_2 nanosheets in the aqueous dispersion was measured using DLS. As shown in Fig. 3d, the hydrodynamic size of the MoS_2 nanosheets is mainly in the range of 100-500 nm. We also generated statistical data on the lateral size of the MoS_2 in the aqueous dispersions based on TEM and SEM studies (Fig. S1 in ESI†). The results are comparable to the DLS results.

The Raman spectra of both bulk MoS_2 powder and exfoliated MoS_2 nanosheets are shown in Fig. 4a. Both spectra show the well-known high energy A_{1g} mode (stretching of the sulfur atoms) and lower energy E^1_{2g} (in-plane bending) mode.[9] The

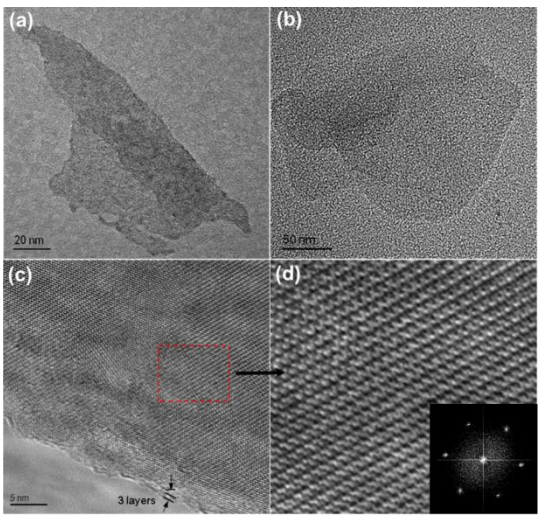

Fig. 2 (a, b) Typical TEM images of exfoliated MoS_2 nanosheets. (c, d) High-resolution TEM image of a tri-layer MoS_2 nanosheet. The inset in (d) is the corresponding SAED pattern.

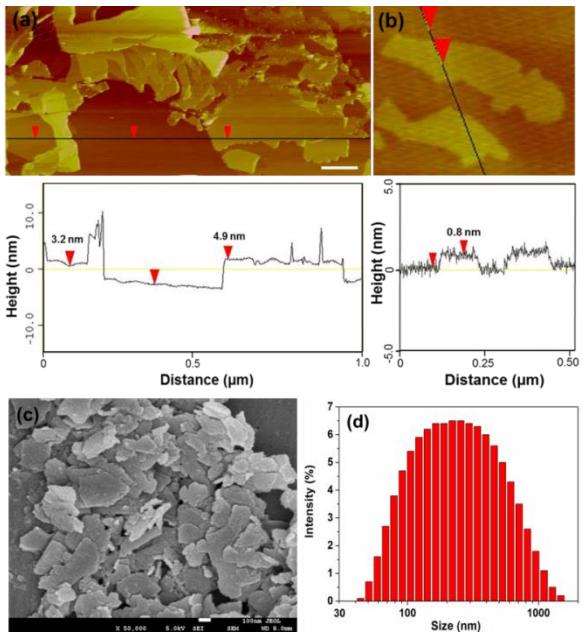

Fig. 3 AFM images (including corresponding height profiles below) of few-layered (a) and monolayer MoS_2 (b) nanosheets. (c) SEM images of exfoliated MoS_2 powder. (d) Hydrodynamic size distribution of the exfoliated MoS_2 nanosheets (sonication time = 80 h). The scale bars in (c) is 100 nm.

E^1_{2g} and A_{1g} peaks show red-shifts from 383 and 409 cm^{-1} for the bulk MoS_2 to 381 and 407 cm^{-1} for the exfoliated MoS_2. Typically, compared with bulk MoS_2, the A_{1g} mode of the exfoliated MoS_2 shows a red-shift due to the deceased interlayer Van der Waals force while the E^1_{2g} mode shows a blue-shift due to the long-range Coulombic interlayer interactions.[30,31] However, similar to our result, the red-shift of E^1_{2g} mode has also been reported for MoS_2 nanosheets prepared by some chemical-assisted exfoliation or chemical synthesis methods.[3,22,32] In such systems, surfactants, intercalation agents or solvents may be adsorbed on the surface of the MoS_2 nanosheets. Thus, it is believed that in our case, the AL adsorbed on the surface of the exfoliated MoS_2 nanosheets may affect the in-plane atomic bending vibration, which is related to the behavior of E^1_{2g} mode.

The XRD patterns of the bulk and exfoliated MoS_2 are shown in Fig. 4b. All the diffraction peaks are consistent with the hexagonal 2H-MoS_2 (JCPDS: 65-1951), except a much reduced peak density of (002) reflection for the exfoliated MoS_2, indicating the successful exfoliation of MoS_2. Finally, XPS spectrum of the exfoliated MoS_2 nanosheets (Fig. 4c) shows two Mo 3d peaks which can be assigned to Mo^{4+} $3d_{5/2}$ (229.4 eV) and Mo^{4+} $3d_{3/2}$ (232.5 eV). Almost no trace of Mo^{6+} $3d_{5/2}$ peak (~236 eV) was observed, indicating oxidation didn't occur during the treatment.

3.2. Exfoliated MoS_2 nanosheets as LIB electrode materials

Graphene-like MoS_2 has been explored as lithium-ion host materials because its high reversible capacity and rate capability, whereas these monolayer and multilayer MoS_2 nanosheets were mainly synthesized by bottom-up approaches, such as hydrothermal, pyrolysis and CVD.[33-35] The facile aqueous exfoliation method described above has the potential for large scale preparation of MoS_2 nanosheets from low-cost MoS_2 mineral. Different from the aforementioned methods, this

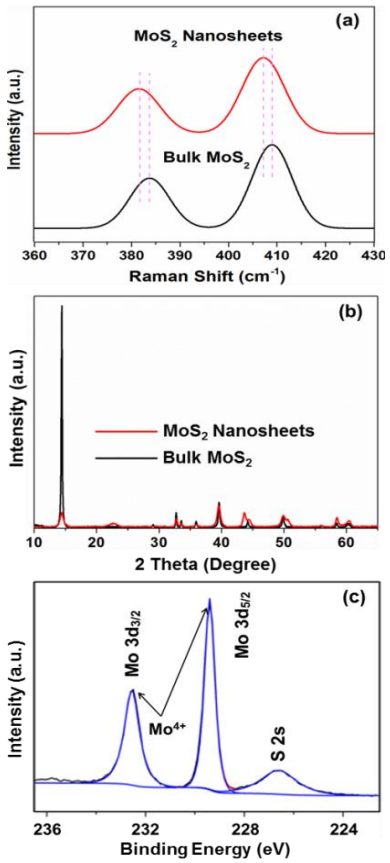

Fig. 4 (a) Raman spectra and (b) XRD patterns of bulk MoS_2 and exfoliated MoS_2 nanosheets. (c) Mo 3d XPS spectrum of the exfoliated MoS_2 nanosheets after annealing.

top-down method preserves the pristine structure of MoS_2. However, the electrochemical behaviors of pristine MoS_2 nanosheets have not been studied so far, to the best of our knowledge. Thus in this work, the exfoliated MoS_2 nanosheets were studied as lithium-ion host materials in LIBs.

Although most of the current work on MoS_2 for LIBs is focused on the use of MoS_2 as anodes, MoS_2 cathode is an emerging and highly promising area that needs to be paid special attention.[36] The CV curves of the exfoliated MoS_2 nanosheet are shown in Fig. 5a. In the first cycle, the sharp cathodic peak at 1.07 V is attributed to the insertion of Li^+ into the MoS_2 layer, accompanied by a phase change from 2H to 1T with Li^+ occupying the interlayer S−S tetrahedron site.[37] While the anodic doublet at around 2 V is assigned to the extraction of Li^+ from the lattice of 1T-MoS_2.[38] Therefore, the Li^+ insertion is highly reversible in this range. It is interesting that two small cathodic peaks at 1.58 and 1.29 V are also observed, indicating a stepwise transition may occur due to the presence of ultra-thin nanosheets.[39,40] Their corresponding anodic peaks are found at 1.69 V and 1.40 V, with a ΔV of 0.18 V. These peaks are absent for the pristine MoS_2 sample (Fig. S2 in ESI†).

The first 3 discharge-charge curves in the potential range between 1 and 3V were shown in Fig. 5b. The initial charge capacity is 196 mAh g^{-1} at 0.1C (1C = 167 mAh g^{-1}) with a Coulombic efficiency (CE) as high as 85%. In the following cycles, the CE quickly stabilized at 100% and a reversible capacity of 164 mAh g^{-1} is reached at the 40th cycle (Fig. 5c). The exfoliated MoS_2 nanosheets exhibit excellent rate

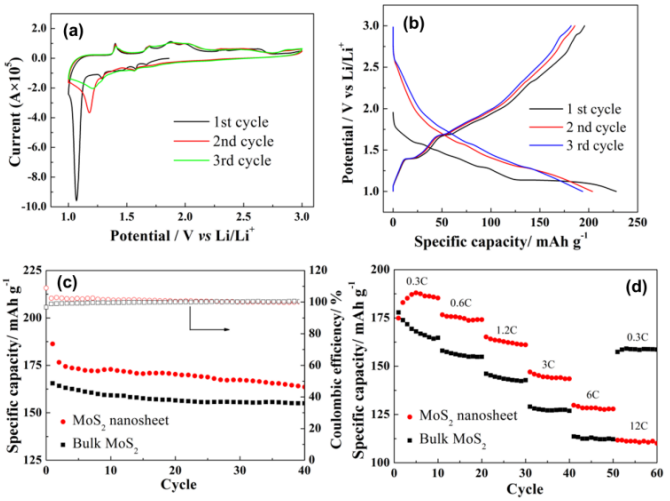

Fig. 5 (a) Cyclic voltammograms, (b) discharge−charge profiles at 0.1C, (c) cycling performance at 0.6C and (d) rate capabilities of the exfoliated MoS_2 nanosheets between 1-3V.

capability compare to its bulk counterpart (Fig. 5d). The reversible capacities at 0.3C, 0.6C, 1.2C, 3C and 6C are 185, 175, 160, 144 and 128 mAh g^{-1}, respectively. The capacity maintains above 110 mAh g^{-1} even at 12C, which is 60% retention of the highest capacity corresponding to 3 min charge/discharge. This outstanding performance could be explained by the ultra-thin nature of MoS_2 nanosheet, which greatly increases the contact surface area with electrolyte and shortens the electron and ion migration length. The relatively smaller lateral size of MoS_2 nanosheets may also contribute to the high capacity and rate capability because more edge sulfur atoms are exposed as redox centers.[41] The variation in electrode composition has little effect on the electrochemical performance, as shown in Fig. S3 (see ESI†). After 100 cycles, the reversible capacity is still above 110 mAh/g at 1C with 10 wt% carbon black only. Given the facile and scalable fabrication process, it is believed that this exfoliated MoS_2 nanosheet could be a promising cathode material for low-cost LIBs.[36]

A significant change in lithiation mechanism will occur when the MoS_2 cell is further discharged,[42,43] as shown in Fig. 6a. Below 1 V, the broad shoulder peak at around 0.69V corresponds to the insertion of additional Li^+ into the ultrathin MoS_2 nanosheets.[43] The distinct peak at 0.47 V is derived from the conversion reaction from 1T-MoS_2 to Mo/Li_2S. In the anodic scan, the intensive peak at 2.32 V is associated with the oxidation of Li_2S to S. It is worth noting that, the 1.58/1.70 V and 1.29/1.41 V redox couples are again observed and their intensities decrease with cycling, indicating the conversion reaction between MoS_2 and Li_2S/Mo is partially reversible.[44-46] In the second discharge, the cathodic peak at 1.90 V is attributed to the lithiation of S. The weak peaks at 1.07 V and 0.35 V can be assigned to the lithiation of the re-formed MoS_2 followed by decomposition of the lithiated MoS_2. The electrochemical performances of the exfoliated MoS_2 nanosheet as an anode are shown in Fig. 6b-d. The initial charge and discharge capacities are 838 and 1022 mAh g^{-1}, respectively, with a CE of 82%. This higher CE is ascribed to the fast ion/electron transport of the ultrathin MoS_2 nanosheets.[47-49] The reversible capacity increases gradually in the beginning until the 12th cycle (970 mAh g^{-1}) and maintains above 600 mAh g^{-1} at the 50th cycle. The exfoliated MoS_2 nanosheets deliver

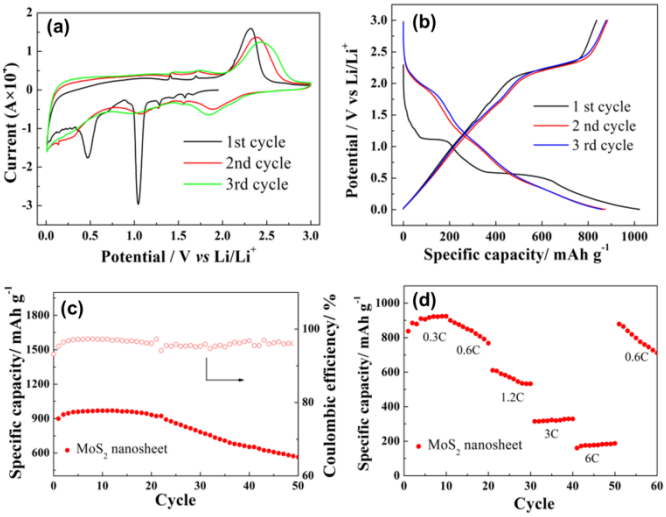

Fig. 6 (a) Cyclic voltammograms, (b) discharge–charge profiles at 0.3C, (c) cycling performance at 0.6C and (d) rate capabilities of the exfoliated MoS_2 nanosheets between 0.01-3V.

reversible capacities of 920, 800, 550, 330 and 190 mAh g^{-1} at 0.3C, 0.6C, 1.2C, 3C and 6C respectively. The reversible capacity restores to ca. 750 mAh g^{-1} when the current density is reset to 0.6C.

3.3. AL-assisted exfoliation of other types of layered materials in water

Other than MoS_2, AL also shows strong stabilizing effects in exfoliating other layered crystals in water. Our recent publication has demonstrated the exfoliation of graphite in water with the assistance of AL (Fig. 7a).[50] Herein we also demonstrate that AL can effectively assist the exfoliation of WS_2 and BN in water and stabilize the exfoliated nanosheets (Figs. 7b and 7c). We also measured the size distributions of WS_2 and BN nanosheets in the aqueous dispersions by DLS, as shown in Fig. S4 in ESI†. The mean hydrodynamic sizes of the exfoliated WS_2 and BN nanosheets are 285.2 and 530.5 nm, respectively. The concentrations of the WS_2 and BN aqueous dispersions are 0.19±0.03 and 0.11±0.02 mg mL^{-1}, respectively. The above results demonstrate that the low cost, non-toxicity and superior surfactant performance of AL make it an attractive candidate for economical and eco-friendly production of a wide range of two-dimensional nano-materials. Further optimization of dispersing parameters for WS_2 and BN will be conducted. More details about AL-assisted exfoliation of WS_2, BN and other layered materials as well as their applications will be reported in future publications.

4. Conclusions

AL has been successfully used as surfactant to produce MoS_2 nanosheets in aqueous media by liquid-phase exfoliation method. It exhibits excellent stabilizing function for the exfoliated MoS_2 nanosheets. With optimized dispersion parameters, the MoS_2 concentration of the resulting dispersion can reach 1.75±0.08 mg mL^{-1}. The stabilization mechanism lies in the electrostatic repulsion between negative charged AL as well as the steric hinerance of AL macromolecule. Microscopy study shows that the majority of the exfoliated MoS_2 nanosheets have only few layers with lateral size of 100 - 500 nm. Excellent rate capability is achieved when the exfoliated

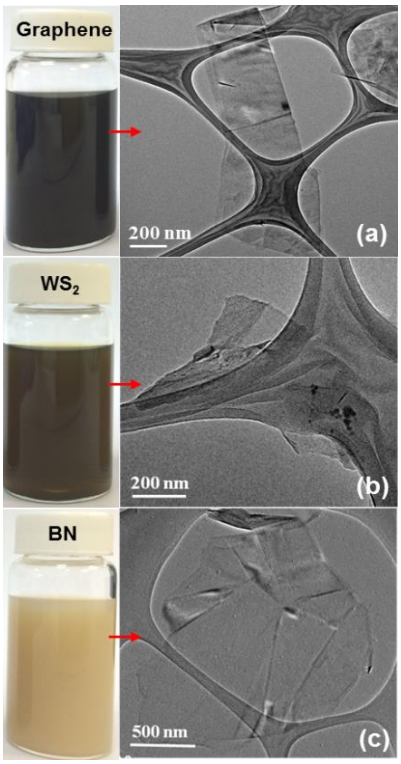

Fig. 7 Photographs of aqueous dispersions and representative TEM images of the exfoliated nanosheets. (a) AL-graphene aqueous dispersion was prepared as described in our previous work.[49] (b) AL-WS_2 and (c) AL-BN aqueous dispersions were prepared by ultrasonic treatment for 5 h and centrifugation at 2000 rpm for 1 h. The concentration of AL was 0.5 mg mL^{-1}. The feed contents of bulk WS_2 and BN were 5 mg mL^{-1}.

MoS_2 nanosheets are used as cathode in LIBs. The capacity maintains above 110 mAh/g at 12C, showing great promise as an alternative low-cost LIB cathode material. When the exfoliated MoS_2 nanosheets are used as an anode, the LIB cells show relatively good capacity retention. Finally, it is demonstrated that AL has great potential to be a versatile surfactant for exfoliation of other types of layered materials, including graphite, WS_2 and BN. It shows that lignin is an extremely versatile surfactant and may have great potentials for high value-added products in many fields.

Acknowledgements

Chenyang Zhao thanks Nanyang Technological University, Singapore, for providing him a Ph.D. scholarship in the course of this work.

Notes and references

[a] School of Materials Science and Engineering, Nanyang Technological University, 50 Nanyang Avenue, Singapore 639798, Singapore. E-mail: asxhlu@ntu.edu.sg

[b] Institute of Materials Research and Engineering, A*STAR (Agency for Science, Technology and Research), 3 Research Link, Singapore 117602, Singapore.

† Electronic Supplementary Information (ESI) available: [CV of the bulk MoS_2 between 1-3V, electrochemical performances of the exfoliated MoS_2 nanosheets between 1-3V with 10 wt% carbon black, referenced

table of exfoliation of MoS_2 in aqueous media.]. See DOI: 10.1039/b000000x/

‡ These authors contributed equally to this work.

1 Q. H. Wang, K. Kalantar-Zadeh, A. Kis, J. N. Coleman and M. S. Strano, *Nat. Nanotechnol*., 2012, **7**, 699-712.

2 K. F. Mak, C. Lee, J. Hone, J. Shan and T. F. Heinz, *Phys. Rev. Lett*., 2010, **105**, 136805.

3 H. S. S. R. Matte, A. Gomathi, A. K. Manna, D. J. Late, R. Datta, S. K. Pati and C. N. R. Rao, *Angew. Chem. Int. Ed*., 2010, **49**, 4059-4062.

4 L. Zhang, H. B. Wu, Y. Yan, X, Wang and X. W. Lou, *Energy Environ. Sci*., 2014, **7**, 3302–3306.

5 M. Bernardi, M. Palummo and J. C. Grossman, *Nano Lett.*, 2013, **13**, 3664-3670.

6 B. Radisavljevic, A. Radenovic, J. Brivio, V. Giacometti and A. Kis, *Nat. Nanotechnol*., 2011, **6**, 147-150.

7 B. Radisavljevic, M. B. Whitwick and A. Kis, *ACS NANO*, 2011, **12**, 9934-9938.

8 J. Zhang, S. Najmaei, H. Lin and J. Lou, *Nanoscale*, 2014, **6**, 5279–5283.

9 M. D. J. Quinn, N. H. Ho and S. M. Notley, *ACS Appl. Mater. Interfaces*, 2013, **5**, 12751-12756.

10 A. Winchester, S. Ghosh, S. Feng, A. L. Elias, T. Mallouk, M. Terrones and S. Talapatra, *ACS Appl. Mater. Interfaces*, 2014, **6**, 2125-2130.

11 K. Chang and W. Chen, *ACS NANO*, 2011, **5**, 4720-4728.

12 L. Cao, S. Yang, W. Gao, Z. Liu, Y. Gong, L. Ma, G. Shi, S. Lei, Y. Zhang, S. Zhang, R. Vajtai and P. M. Ajayan, *Small*, 2013, **9**, 2905-2910.

13 A. Splendiani, L. Sun, Y. Zhang, T. Li, J. Kim, C. Chim, G. Galli and F. Wang, *Nano Lett*., 2010, **10**, 1271-1275.

14 S. S. Chou, B. Kaehr, J. Kim, B. M. Foley, M. De, P. E. Hopkins, J. Huang, C. J. Brinker and V. P. Dravid, *Angew. Chem. Int. Ed*., 2013, **52**, 4160-4164.

15 J. Zheng, H, Zhang, S. Dong, Y. Liu, C. T. Nai, H. S. Shin, H. Y. Jeong, B. Liu and K. P. Loh, *Nat. Commun*., 2014, **5**, 2995.

16 V. Nicolosi, M. Chhowalla, M. G. Kanatzidis, M. S. Strano and J. N. Coleman, *Science*, 2013, **340**, 1420-1438.

17 A. Castellanos-Gomez, M. Barkelid, A. M. Goossens, V. E. Calado, H. S. J. van der Zant and G. A. Steele, *Nano Lett*., 2012, **12**, 3187-3192.

18 J. Jeon, S. K. Jang, S. M. Jeon, G. Yoo, Y. H. Jang, J. Park and S. Lee, *Nanoscale*, 2015, **7**, 1688-1695.

19 R. J. Smith, P. J. King, M. Lotya, C. Wirtz, U. Khan, S. De, A. O'Neill, G. S. Duesberg, J. C. Grunlan, G. Moriarty, J. Chen, J. Wang, A. I. Minett, V. Nicolosi and J. N. Coleman, *Adv. Mater*., 2011, **23**, 3944-3948.

20 A. O'Neill, U. Khan and J. N. Coleman, *Chem. Mater*., 2012, **24**, 2414-2421.

21 J. Wang, L. Lu, M. Lotya, J. N. Coleman, S. Chou, H. Liu, A. I. Minett and J. Chen, *Adv. Energy Mater*., 2013, **3**, 798-805.

22 W. Yin, L. Yan, J. Yu, G. Tian, L. Zhou, X. Zheng, X. Zhang, Y. Yong, J. Li, Z. Gu and Y. Zhao, *ACS Nano*, 2014, **8**, 6922-6933.

23 Y. Yao, Z. Lin, Z. Li, X. Song, K. Moon and C. P. Wong, *J. Mater. Chem*., 2012, **22**, 13494-13499.

24 F. G. Calvo-Flores and J. A. Dobado, *ChemSusChem*, 2010, **3**, 1227-1235.

25 T. Saito, J. H. Perkins, F. Vautard, H. M. Meyer, J. M. Messman, B. Tolnai and A. K. Naskar, *ChemSusChem*, 2014, **7**, 221-228.

26 M. Lotya, Y. Hernandez, P. J. King, R. J. Smith, V. Nicolosi, L. S. Karlsson, F. M. Blighe, S. De, Z. Wang, I. T. McGovern, G. S. Duesberg and J. N. Coleman, *J. Am. Chem. Soc*., 2009, **131**, 3611-3620.

27 P. May, U. Khan, J. M. Hughes and J. N. Coleman, *J. Phys. Chem. C*, 2012, **116**, 11393-11400.

28 G. Wang and H. Chen, *Sep. Purif. Technol*., 2013, **105**, 98-105.

29 Z. Zeng, Z. Yin, X. Huang, H. Li, Q. He, G. Lu, F. Boey and H. Zhang, *Angew. Chem. Int. Ed*., 2011, **50**, 11093–11097.

30 H. Li, Q. Zhang, C. C. R. Yap, B. K. Tay, T. H. T. Edwin, A. Olivier and D. Baillargeat, *Adv. Funct. Mater*., 2012, **22**, 1385-1390.

31 C. Lee, H. Yan, L. E. Brus, T. F. Heinz, J. Hone and S. Ryu, *ACS Nano*, 2010, **4**, 2695-2700.

32 A. A. Jeffery, C. Nethravathi and M. Rajamathi, *J. Phys. Chem. C*, 2014, **118**, 1386–1396.

33 C. Zhu, X. Mu, P. A. van Aken and Y. Yu, J. Maier, *Angew. Chem., Int. Ed.*, 2014, **53**, 2152-2156.

34 X. Cao, Y. Shi, W. Shi, X. Rui, Q. Yan, J, Kong and H. Zhang, *Small*, 2013, **9**, 3433-3438.

35 H. Hwang, H. Kim and J. Cho, *Nano Lett*., 2011, **11**, 4826-4830.

36 T. Stephenson, Z. Li, B. Olsen and D. Mitlin, *Energy Environ. Sci*., 2014, **7**, 209-231.

37 L. Wang, Z. Xu, W. Wang and X. Bai, *J. Am. Chem. Soc*., 2014, **136**, 6693-6697.

38 X. Fang, C. Hua, X. Guo, Y. Hu, Z. Wang, X. Gao, F. Wu, J. Wang and L. Chen, *Electrochimica Acta*, 2012, **81**, 155-160.

39 F. Zhou, S. Xin, H. Liang, L. Song and S. Yu, *Angew. Chem., Int. Ed*., 2014, **53**, 11552-11556.

40 U. K. Sen, P. Johari, S. Basu, C. Nayak and S. Mitra, *Nanoscale*, 2014, **6**, 10243-10254.

41 J. Xie, H. Zhang, S. Li, R. Wang, X. Sun, M. Zhou, J. Zhou, X. W. Lou and Y. Xie, *Adv. Mater*., 2013, **25**, 5807-5813.

42 X. Fang, X. Guo, Y. Mao, C. Hua, L. Shen, Y. Hu, Z. Wang, F. Wu and L. Chen, *Chem.-Asian J*., 2012, **7**, 1013-1017.

43 J. Xiao, X. Wang, X. Yang, S. Xun, G. Liu, P. K. Koech, J. Liu and J. P. Lemmon, *Adv. Funct. Mater*., 2011, **21**, 2840-2846.

44 J. Wang, J. Liu, D. Chao, J. Yan, J. Lin and Z. X. Shen, *Adv. Mater*., 2014, **26**, 7162-7169.

45 J. Kong, C. Zhao, Y. Wei, S. L. Phua, Y. Dong and X. Lu, *J. Mater. Chem. A*, 2014, **2**, 15191-15199.

46 X. Fang, X. Yu, S. Liao, Y. Shi, Y. Hu, Z. Wang, G. D. Stucky and L. Chen, *Microporous Mesoporous Mater*., 2012, **151**, 418-423.

47 C. Zhao, J. Kong, X. Yao, X. Tang, Y. Dong, S. L. Phua and X. Lu, *ACS Appl. Mater. Interfaces*., 2014, **6**, 6392-6398.

48 C. Zhao, J. Kong, L. Yang, X. Yao, S. L. Phua and X. Lu, *Chem. Commun*., 2014, **50**, 9672-9675.

49 K. Chang and W. Chen, *Chem. Commun*., 2011, **47**, 4252-4254.

50 W. Liu, R. Zhou, D. Zhou, G. Ding, J. M. Soah, C. H. Yue and X. Lu, *Carbon*, 2015, **83**, 188-197.